Journal of Applied Polymer Science

Polyaniline self-assembled with DTPA: Facilely tuned morphology and properties

Mohammed Gibreel,[1] Xinli Jing,[2] Yu Li,[2] Yongzhong Liu[1]

[1]Department of Chemical Engineering, School of Chemical Engineering and Technology, Xi'an Jiaotong University, Xi'an 710049, People's Republic of China

[2]Department of Applied Chemistry, School of Science, Xi'an Jiaotong University, Xi'an 710049, People's Republic of China

Correspondence to: Y. Li (E-mail: yuli2012@mail.xjtu.edu.cn)

ABSTRACT: The effects of pH profile and "soft template" during aniline chemical oxidative polymerization (COP) were investigated and evaluated simultaneously with diethylene triamine pentaacetic acid (DTPA) as a structural directing agent. Formation of PANI nanotubes and nanoparticles, smooth microspheres, and urchin-like microspheres were illustrated by evaluating the pH profile during aniline COP while considering the "soft template" effects of DTPA. PANI nanosheets with two semicurled edges were found in the system producing nanotubes, which provides an evidence for the "curling mechanism" of PANI nanotube formation. With different pH profiles, chemical structures and aggregation structures of the as-synthesized PANI micro/nanostructures are similar, whereas their conductivity, wettability, Cr (VI) adsorption, and electrochemical behaviors are distinct. The present study indicates that if properly conducted, pH profile adjustment is more effective than "soft template" to control the morphology and to optimize the performance of PANI micro/nanostructures. © 2015 Wiley Periodicals, Inc. J. Appl. Polym. Sci. **2015**, *132*, 42403.

KEYWORDS: conducting polymers; nanostructured polymers; self-assembly

Received 25 November 2014; accepted 22 April 2015

DOI: 10.1002/app.42403

INTRODUCTION

Conducting polymers, such as polyaniline (PANI), have stand out as one of the most important materials in current years due to their attractive electrical/optical properties, and remarkable advantages like easy synthesis, excellent environmental stability, and simple acid doping–base dedoping process.[1,2] Moreover, PANI has the ability to self-assemble into various micro/nanostructures during the chemical oxidative polymerization (COP) of aniline (Ani), which is very easy to manipulate and offering lots of possibilities to tune the formation of PANI micro/nanostructures. Generally, variation of dopant acid, oxidant, molar ratio of aniline to the oxidant, pH of the reaction medium, feed ways of the reactants,[3–10] or external interference will all induce morphology changes of PANI micro/nanostructures.[11,12] It has been found that the performance of PANI micro/nanostructures is highly dependent on their morphologies, thus study on morphology control and performance improvement of self-assembled PANI remains the most challenging work in this field.

In early days, "hard" and "soft" templates were employed to shape the morphology of PANI, whereas in recent years, PANI was found to be able to assemble into multidimensional supramolecular structures by themselves. Though the self-assembly approaches give a chance to acquire PANI micro/nanostructures getting rid of any "hard" or "soft" templates, their reproducibility is poor, and the products usually lose uniformity due to continuously changing reaction medium conditions. In the case of "soft template", the exact roles of organic functional acids, surfactants, or ionic liquids played on the formation of PANI micro/nanostructures are still not very clear. As a matter of fact, in a typical aniline COP system with ammonium peroxydisulfate (APS) as the oxidant, hydrogen ions and SO_4^{2-} ions are gradually released as the polymerization progresses, leading to formation of H_2SO_4 whose acidity is stronger than most organic acids. Since the SO_4^{2-} ions are much smaller than counter anions of common surfactants or ionic liquids, it makes them easily incorporated into PANI chains and electrostatic interaction is usually 2 or 3 magnitudes higher than other noncovalent interactions, the polymerization products will probably interact with H_2SO_4 excessively even in an aniline COP system without any external dopant acids. The presence of sulfur in PANI backbone has been widely reported.[13–15]

With this consideration, we are motivated to get a closer sight on the effects of "soft template" with variable pH profiles, in order to

Additional Supporting Information may be found in the online version of this article.

reveal how these factors work during the formation of PANI micro/nanostructures. With three nitrogen atoms and five carboxyl groups, diethylene triamine pentaacetic acid (DTPA) provides many noncovalent interaction sites and has been widely used as a strong chelating agent to heavy metal ions. In our case, DTPA was chosen as a structure directing agent, and the hydrogen bonding and electrostatic interaction between DTPA and PANI as well as a quasi-steric configuration of DTPA (Supporting Information, Scheme 1) are expected to manifest the role of "soft template" sufficiently. Besides, PANI has been widely reported as a promising candidate adsorbent for removal of toxic metal ions such as Cr (VI) from aqueous medium,[16–20] and DTPA is well known as a strong chelating agent; it is supposed that PANI micro/nanostructure with DTPA incorporated and possessing a large specific surface area will be efficient for removal of heavy metal ions from water. According to our knowledge, though there have been a lot of reports on PANI micro/nanostructures synthesized with "soft templates", few works have been published on the formation of PANI micro/nanostructures in the presence of DTPA.

Herein, aniline COP was carried out with three kinds of pH profiles achieved by adjusting the concentration of aniline and its molar ratio to DTPA. The structure and performance of the as-produced PANI micro/nanostructures were analyzed and evaluated carefully to elucidate the roles played by "soft template" under different pH profiles. It has been found that the "soft template" effect of DTPA seems to be weakened with rapidly dropped pH or at a higher acidity level, and morphology evolution of aniline products is more sensitive to the pH profile. Owing to their diverse construction environment, the PANI micro/nanostructures show distinct performances which make them attractive materials.

EXPERIMENTAL

Materials

All the chemicals with analytic purity were from the Xi'an Chemical Reagent Factory. Aniline monomer was distilled under reduced pressure in the presence of zinc powder and kept in a freezer before use; and the others were used as received without further purification.

Synthesis of PANI Micro/Nanostructures

In a typical synthesis procedure for PANI–DTPA, which showed nanotubes morphology, 0.0944 g (0.24 mmol) of DTPA was dissolved in 20 mL of deionized water at room temperature. This solution was divided into two portions (about 15 and 5 mL); 0.1118 g (1.2 mmol) of aniline monomer and 0.2738 g (1.2 mmol) of APS were dissolved in the 15 and 5 mL of DTPA solutions, respectively. The aniline solution and APS solution were placed in a water bath until their temperatures reached 25°C. Then, the two solutions were rapidly mixed at once, sufficiently stirred for a few minutes, and then placed in the water bath undisturbed for 24 h. Finally, the resulting precipitate was collected in a filter, washed repeatedly with distilled water until the filtrate became colorless, and then dried in vacuum at 45°C for 4–5 h. In this synthetic procedure, the [Ani] was 0.06 M and aniline-to-acid ratio [Ani]/[DTPA] was 5 : 1. Other samples were synthesized by a similar method and in all reaction systems, the molar ratio of APS to aniline was set as 1 : 1.

Measurement and Characterization

pH and Morphology. During the polymerization, evolution of reactions acidity was recorded by a pH meter (PHSJ-4A, Shanghai Precision & Scientific Instruments Co., Ltd, China). The morphologies of as-synthesized products, in their doped state, were characterized by scanning electron microscopy (SEM, FEI Quanta F250) directly using the dried sample powder and by transmission electron microscopy (TEM, JEM–200CX, JEOL) after samples have been dispersed in deionized water.

Structure. The structures of as-synthesized products were characterized by Fourier transform infrared (FTIR) spectroscopy, X-ray diffraction (XRD), ultraviolet–visible (UV–vis) spectroscopy, and X-ray photoelectron spectra (XPS). FTIR spectra of the dried samples, in the range of 4000–400 cm^{-1}, were recorded using a Bruker Tensor 27 spectrometer. The dried samples were mixed with potassium bromide (KBr) and finely ground using a mortar and pestle and then pressed into pellets or disks. UV–vis spectra for dispersed samples in deionized water were recorded with a UV2550 (Shimadzu) spectrometer. XRD patterns were collected on an XRD-D8 diffractometer (ADVANCE Bruker). XPS was recorded with the totally dried samples on a Thermo Scientific K-Alpha X-ray photoelectron spectrometer with an (AlK_{α}) source.

Conductivity. Conductivity test was carried out on a four-point probe (SZ85 digital multimeter, Suzhou Telecommunication Factory, China) using the pressed pellets of the thoroughly dried sample (*ca* 12 mm in diameter and 0.7 mm in thickness).

Wettability. The wettability of the products was evaluated by measuring the static contact angles (CA) with approximately 5 μL of water using a DSA 100 (Krüss, Germany) apparatus. CA measurements were determined by slowly tilting the samples until the drops started moving. Each of the reported CA values represents the average of six measurements.

Electrochemical Behavior. The electrochemical test was performed on a CHI 660 E electrochemical workstation using a three-electrode cell system in 1 M H_2SO_4 with a Pt foil as the counter electrode and a saturated calomel electrode (SCE) as the reference electrode, respectively. The working electrode was prepared by mixing the as-prepared PANI powder with carbon black and polyvinylidene fluoride (PVDF, 5 wt % solution in NMP) into slurry at a mass ratio of 7 : 2 : 1, followed by pasting the slurry onto a carbon paper (1 × 1 cm) and then drying under vacuum at 60°C for 4 h. The capacitance properties were studied by galvanostatic charge/discharge and cyclic voltammetry (CV) tests, according to the following formula:

$$C = \frac{I \cdot \Delta t}{\Delta V \cdot m} \quad (1)$$

Where I is the discharge current (A), Δt is the discharge time (s), ΔV is the voltage differences during the discharge process (V), and $m$is the mass of the active material.

Removal of Chromium (VI). Standard solutions of Cr (VI) with different concentrations (5, 10, 30, 50, 70, and 80 ppm) were prepared by dissolving a precisely weighted amount of

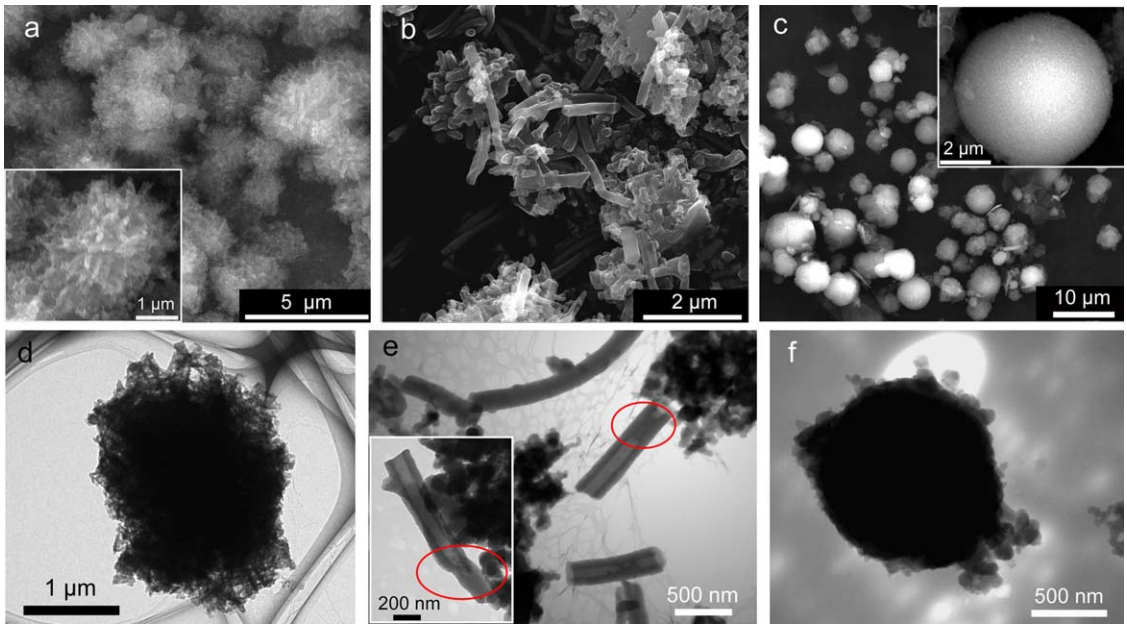

Figure 1. Typical (a–c) SEM and (d–f) TEM images of PANI micro/nanostructures obtained with the molar ratio of [Ani]/[DTPA] = 5 : 1 (a, b, d, e) and 1 : 1 (c, f). (a,d): urchin-like PANI microspheres, [Ani]/[DTPA] = 5 : 1, [Ani] = 0.01 M; (b,e): nanotubes mixed with nanoparticles, [Ani]/[DTPA] = 5 : 1, [Ani] = 0.06 M; (c,f): smooth PANI microspheres, [Ani]/[DTPA] = 1 : 1, [Ani] = 0.007 M. The inserts are the corresponding micro/nanostructures with higher magnifications. [Color figure can be viewed in the online issue, which is available at wileyonlinelibrary.com.]

potassium dichromate ($K_2Cr_2O_7$) in 100 mL of deionized water by the method of serial dilution. A standard curve correlates the concentration of Cr (VI) and the absorbance at λ_{max} (353 nm) was obtained by recording the UV–vis absorption of Cr solution. Cr solution of 25 ppm was used for detecting the adsorption ability of PANI.

The adsorption experiments were carried out by adding 0.01 g of dried as-synthesized PANI into 10 mL from 25 ppm of Cr (VI) solution at pH = 1 (adjusted by dilute H_2SO_4) under room temperature. The mixture was ultrasonically treated for 1 h and then kept at room temperature for 3 h. Then the mixture was centrifuged (at 10,000 rpm for 3 min) and the supernatant liquid was used for analyzing the final Cr (VI) concentration by recording their absorbance at the wavelength of 353 nm. Then the removal percentage (R) of the used polymer was calculated as well, using the following equation:

$$R = \frac{C_i - C_f}{C_i} \times 100\% \quad (2)$$

Where C_i and C_f are the initial and final concentrations of Cr (VI), respectively. As control, PANI micro/nanostructures redoped with DTPA were used as the adsorbent under the same condition.

RESULTS AND DISCUSSION

Morphology Control with Different pH Profiles

The aniline COP products display morphology evolution from urchin-like microspheres to clusters of nanotubes and nanoparticles with increased initial [Ani] while the molar ratio of [Ani]/[DTPA] is maintained as 5 : 1. When the [Ani] was in the range of 0.005–0.03 M, the final products mainly presented as microspheres with diameters of 2–3 μm. The TEM image showed that this kind of microsphere was solid in center with lots of short nanofibers and small nanoflakes grown on its periphery, which made it looks like a sea-urchin [Figure 1(a,d); Supporting Information, SI, Figure S1]. At an aniline concentration around 0.03 M, the products are more like clusters of short nanofibers (Supporting Information, Figure S1,c). When the [Ani] was further increased to 0.06 M, irregular aggregates composed of nanotubes and nanoparticles (referred as NT and NP) instead of urchin-like microspheres were obtained [Figure 1(b,e)].

The pH profiles of aniline COP systems are helpful for explaining the morphology changes of PANI mentioned above. As shown in Figure 2, the initial pH values of systems *a* and *b* were close, whereas pH in system *a* dropped quickly in the first 40 min and decreased to 1.68 at 240 min, as a much higher aniline concentration facilitated a faster polymerization rate and consequently rapid release of hydrogen ions. This quickly dropped pH may lead to the majority of products formed at a low pH level, so 1-D products co-existing with irregular nanoparticles became the main product.[9,21,22] As a comparison, pH in system *b* decreased gently throughout the whole polymerization course. It is probably that, on one hand, most of the early products in system *b* formed with pH > 3.2, where the less protonated aniline monomers will participate in *ortho*-coupling to form hydrophobic polymerization products, which are prone to organize into spherical particles to minimize their surface energy[8,9,11]; on the other hand, a slowly proceeded polymerization may facilitate self-assembly of products with DTPA to shape PANI[15,23–25] into quasi-spherical structures based on the steric configuration of DTPA–aniline complex (Supporting Information, Scheme 1). With a much lower pH level (*ca* 2.0)

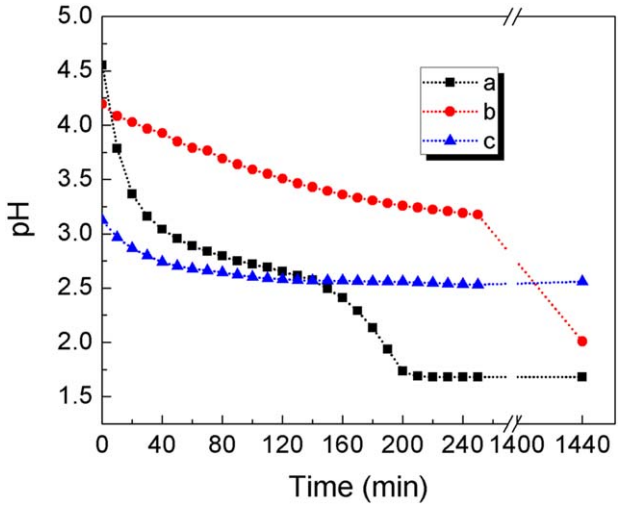

Figure 2. Acidity profiles of the three typical aniline COP systems which produce (a) NT and NP, (b) urchin-like microspheres, and (c) smooth microspheres. a: [Ani] = 0.06 M and [Ani]/[DTPA] = 5 : 1; b: [Ani] = 0.01 M and [Ani]/[DTPA] = 5 : 1; c: [Ani] = 0.007 M and [Ani]/[DTPA] = 1 : 1. [Color figure can be viewed in the online issue, which is available at wileyonlinelibrary.com.]

in the late reaction stage, nanofiber-like products usually appeared in a much stronger acidic system will form and grow onto the earlier formed spherical nucleates,[9,21] finally leading to sea urchin-like microspheres.

Besides systems with pH profiles rapidly decreased below 2.0 or mainly above 3.0, another system with pH level maintained around 2.5 [Figure 2(c)] was designed. Under this condition, DTPA is highly excessive to aniline regarding its functional groups. Microspheres obtained in this case have few small particles and wrinkles on their surfaces, making them look more smooth (referred as "smooth microspheres", Figure 1(c,f); Supporting Information, Figure S2). It can be said that most of the early stage products formed with $2.5 < pH < 3.2$ and the subsequent products formed with pH of *ca* 2.5; this narrow pH variation consequently led to much uniform microspheres [Figure 1(c); Supporting Information, Figure S2].

Formation of these smooth microspheres at pH level around 2.5 can be mainly attributed to the presence of DTPA, which is easy to display a 3-D steric configuration and form pseudospherical complex with aniline (Supporting Information, Scheme 1). In system *c* which yields smooth microspheres, the situation in the early reaction stage may be similar to what happened in system *b* (as discussed above); whereas in the late reaction period, since the pH did not drop a lot to ensure large-scale production of *para*-coupled polymer chains constructing 1-D nanostructures [Figure 2(c)], only tiny wrinkles and small particles formed onto the microspheres. So, with DTPA as the structure directing agent, we have a further understanding that the pH profile (as our group previously reported[9]) as well as the interaction between aniline monomer and the dopant contributes to construction of PANI micro/nanostructures.

Moreover, it should be noticed that in the system with [Ani]/[DTPA] = 5 : 1 and [Ani] = 0.06 M, besides nanorods and nanoparticles, nanotubes with a semicurled structure co-existed [Figure 1(e)]. The circled area in Figure 1(e) shows a 1-D structure with different contrast between its edge and center parts, which was probably originated from a nanosheet with two curled sides. This phenomenon indicates a transition from a nanosheet to a tubular nanostructure. Huang and Li[26] first reported the curling mechanism of PANI nanotubes in the aniline COP system containing methanol, whereas TEM image provided in their work just showed leaf-like structure, which is different from our result. Later, Zujovic and Laslau *et al.*[27,28] developed the curling mechanism based on a "falling pH" aniline COP process in an aqueous system. They proposed that the nanosheets start to curl from one edge and further roll into a tubular structure, where the curling ability is determined by the thickness of PANI nanosheets or nanoflakes. In our case, it seems that the nanosheet is much narrower than that reported by Zujovic *et al.*, and it probably starts to curl from both of its two sides, sealing of the two edges finally gives a tubular structure. Nevertheless, the curling mechanism of PANI nanotubes still needs further investigation.

Structural Analysis

Structural study on the products from systems a, b, and c demonstrates that NT and NP, urchin-like microspheres, and smooth microspheres display the common characters of "standard" PANI except for some tiny distinctions. For instance, in the FTIR spectra (Figure 3), the absorbance bands belong to C═C stretching in quinonoid (Q) rings, (N═Q═N, *ca* 1585 cm^{-1}),[5,6] benzenoid ring (N─B─N, 1502 cm^{-1}), π-electron delocalization induced in the polymer by protonation (1302 cm^{-1}, 1288 cm^{-1}), out-of-plane deformation of C═H in *para*-substituted aromatic ring (~830 cm^{-1})[5,29] all present in the three samples. A characteristic band in protonated PANI

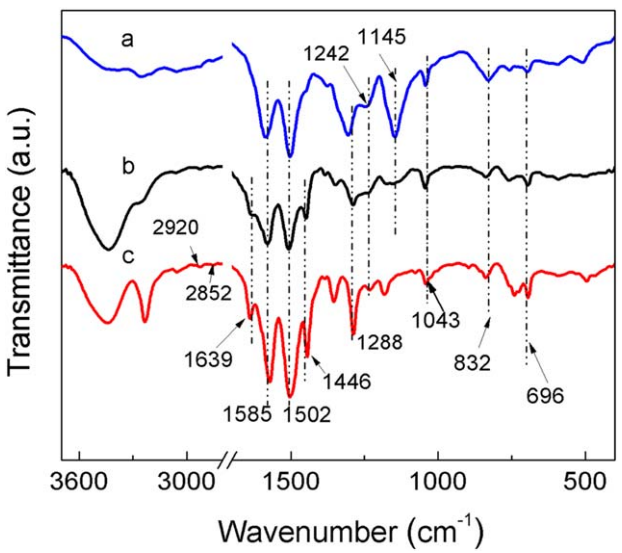

Figure 3. FTIR spectra of as-synthesized products at different [Ani]s and [Ani]/[DTPA] ratios. a: NT and NP, [Ani] = 0.06 M and [Ani]/[DTPA] = 5 : 1; b: urchin-like microspheres, [Ani] = 0.01 M and [Ani]/[DTPA] = 5 : 1; c: smooth microspheres, [Ani] = 0.007 M and [Ani]/[DTPA] = 1 : 1. [Color figure can be viewed in the online issue, which is available at wileyonlinelibrary.com.]

(C—N^+, 1242 cm^{-1}) also can be observed though its intensity is relatively low, indicating that the three samples are doped. Moreover, all products show broad absorption bands in the region of 3400–2800 cm^{-1} (in addition to the band at ~3237 cm^{-1}), which are partially masked by the long absorption tail of the protonated PANI.[30,31] These absorption bands reflect hydrogen bonding and are usually assigned to nitrogen-containing groups, such as secondary amine —NH— and protonated imine —NH^+=.[29]

The NT and NP products displayed a sharp band at 1145 cm^{-1}, which is another character of PANI in doped state, showing its higher protonation degree [Figure 3(a)]. The peaks at 1043 cm^{-1} and 696 cm^{-1} which are untypical for the "standard" PANI can be attributed to the S=O and S—O groups,[14] respectively, probably due to residual sulfate anions and sulfonation of PANI. Nevertheless, Figure 3(c) shows very small peaks at 2920 and 2852 cm^{-1} belonging to the CH_2 group,[32] indicating that a little amount of DTPA may present in the smooth microspheres. A much obvious peak at 1639 cm^{-1} can be ascribed to carboxylic group[24] or C=C stretching vibration in phenazine-like structure induced by *ortho*-coupling.[33] Since in the C1s XPS spectrum of product *c*, no deconvoluted peak belong to O—C=O group can be obtained (Supporting Information, Figure S3), we consider this peak a character of branched units in PANI composed of smooth microspheres. So it can be said that even though aniline COP was carried out in the water solution of DTPA, few DTPA was incorporated into the final product, especially for those obtained in system *a*, which are actually doped with sulfur-containing acid. In comparison with product obtained in system *a*, the bands at 1446 and 1639 cm^{-1} are clearly visible in the spectrum of product *c*, but diminished in intensity in product *b*, indicating presence of

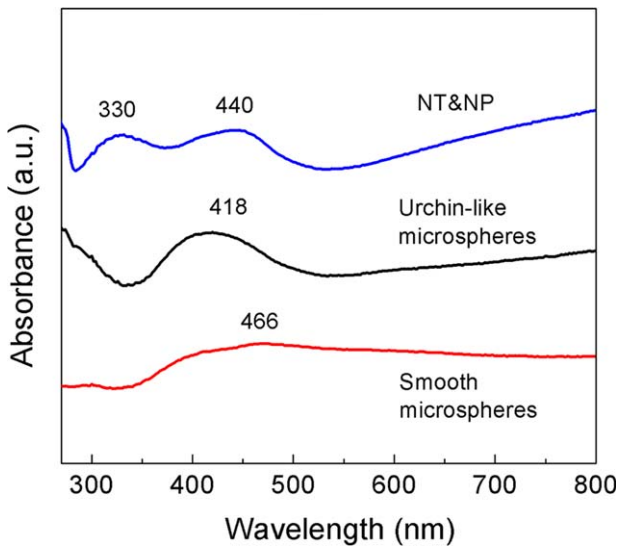

Figure 4. UV–vis absorption spectra of as-synthesized products at different [Ani]s and [Ani]/[DTPA] ratios after dispersed in deionized water. NT and NP: [Ani] = 0.06 M and [Ani]/[DTPA] = 5 : 1; urchin-like microspheres: [Ani] = 0.01 M and [Ani]/[DTPA] = 5 : 1; smooth microspheres: [Ani] = 0.007 M and [Ani]/[DTPA] = 1 : 1. [Color figure can be viewed in the online issue, which is available at wileyonlinelibrary.com.]

Table I. Atomic Concentration (at %) of Three Kinds of PANI Micro/Nanostructures

	NT and NP	Urchin-like microspheres	Smooth microspheres
C	84.32	84.37	81.33
N	4.55	4.84	7.72
O	9.34	9.41	9.61
S	1.8	1.38	1.34
S/N	0.40	0.29	0.17
O/S	5.19	6.82	7.17

ortho-coupled units[9,22,33] in the smooth microspheres and urchin-like microspheres.

The UV–vis spectra show that the NT and NP products possess much well-defined conjugation structure as well as a higher doping degree than the microsphere samples (Figure 4). For instance, the much strong bands located at 330 and 440 nm can be assigned to the π–π^* transition in the benzenoid rings and polaron–π^* transition,[4,33] respectively. A tail appeared starting from 800 nm, which can be attributed to the free carrier tail, indicates more delocalized carrier species in the polymer chains (Figure 4, NT and NP). In the spectrum of urchin-like microspheres, the band corresponding to π–π^* transition disappeared, whereas a strong band belong to polaron–π^* transition appeared at 418 nm, suggesting conjugation defects in the PANI backbone. A slight carrier tail can also be observed around 800 nm, which can be attributed to doped short nanofibers on the periphery of urchin-like PANI microspheres produced in the late polymerization stage with a low acidity (Figure 2). As a comparison, in the spectrum of smooth microspheres, only a weak broad band around 466 nm and the free carrier tail is not obvious, reflecting the serious limitation of carriers' delocalization. The absence of a peak around 800 nm may be due to presence of O=Q=N—, whereas both O and N could be suitable sites for hydrogen bonding.[9,22,27]

A further structural study on these PANI micro/nanostructures was performed with the XPS analysis. The elemental composition shows a C/N ratio which is much higher than the theoretical value of PANI and a significant amount of oxygen (Table I). Since the XPS technique is very sensitive to the surface layer, this result may not be reliable to obtain information of the bulk composition. Also there is a possibility of sample surface contamination as well as hydrolysis of the polymer chains[34,35] during polymerization leading to this high C/N ratio. The presence of sulfur can be ascribed to —SO_3^- and HSO_4^- anions as well as neutral sulfonic acid group —SO_3H according to the S 2p and O 1s high-resolution XPS (Supporting Information, Figures S4 and S5),[36–38] which is in agreement with the FTIR spectra (1040 cm^{-1}, 696 cm^{-1}).[36] These sulfur containing groups may result from decomposition of APS, peroxydisulfate radical attack of the benzene rings, and incomplete hydrolysis of nitrogen or ring-substituted sulfate groups.[39,40] The deconvoluted C 1s spectrum of urchin-like PANI microspheres also showed peak belong to Q=C=O (*ca* 286.5 eV[35]), which is in some level of agreement with the FTIR and UV–vis analysis.

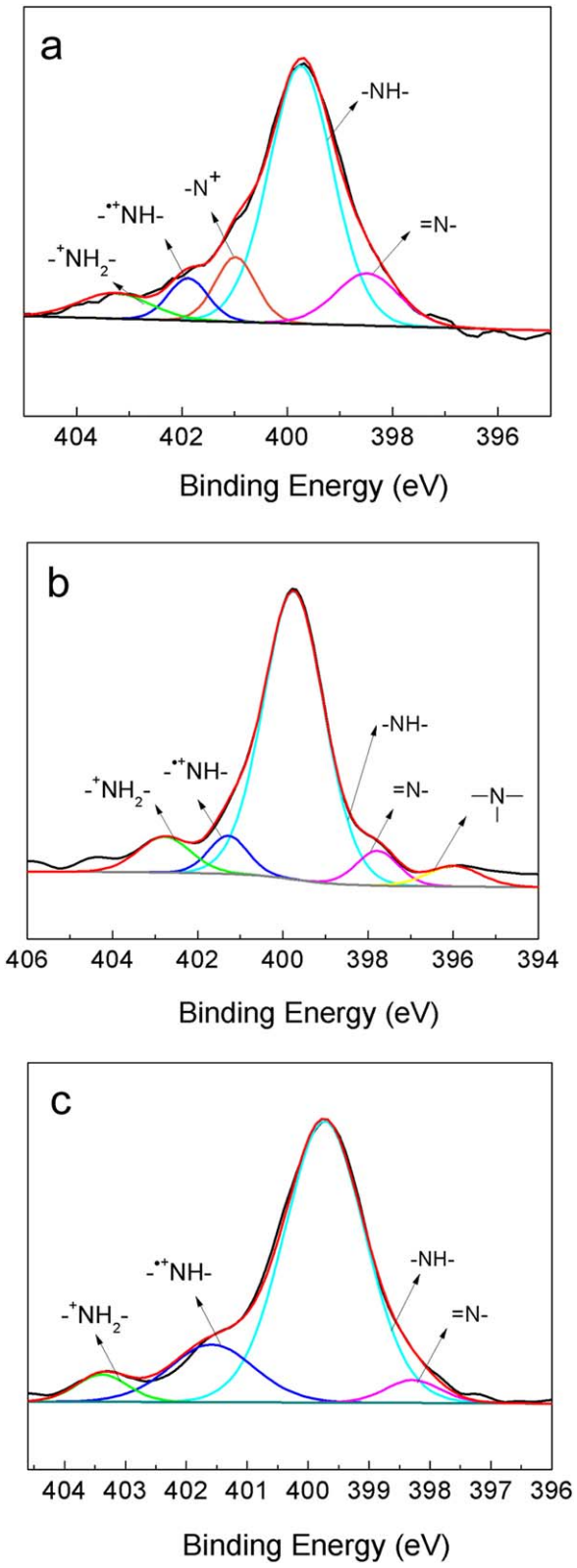

Figure 5. N1s core level XPS spectra of (a) NT and NP, (b) urchin-like microspheres, and (c) smooth microspheres. [Color figure can be viewed in the online issue, which is available at wileyonlinelibrary.com.]

The N 1s core level spectra of the three typical micro/nanostructures are shown in Figure 5. All the three spectra show shoulders at high binding energy besides a symmetrical main peak, indicating the doping of PANI. The peak can be mainly deconvoluted into several chemical environments with their corresponding area ratios shown in Table II. By calculating the percentage of peak area of protonated nitrogen atoms (including —N^+, —$^+$NH—, —$^+NH_2$—),[41] the protonation degree was estimated as 23.60%, 16.37%, and 20.89% for products *a*, *b*, and *c*, respectively. For products *a* and *b*, the protonation degree is lower than their S/N ratios, again indicating that sulfonic groups incorporated into the NT and NP and urchin-like microspheres.[24] In the N 1s spectrum of urchin-like microspheres, one additional shoulder appeared at binding energy of 397.99 eV which can be assigned to three-substituted nitrogen, since its C 1s core level spectrum showed little evidence for the presence of carboxyl group (Supporting Information, Figure S3), we think that the three-substituted nitrogen derives from PANI [Figure 5(b)] other than DTPA. In the system *c*, DTPA is highly excessive to aniline based on its functional groups; it is no wonder that the smooth microsphere sample has much higher nitrogen content and its S/N ratio is lower than its protonation degree. In combination with the FTIR results, it can be said that probably some of the nitrogen-containing groups in the smooth microspheres are doped with DTPA.

The crystallinity of as-prepared products was studied by X-ray diffraction (Figure 6). It can be observed that all products exhibit two broad diffraction peaks centered at 2θ values of 19.1° and 25.6°, which are the characteristic peaks of doped PANI and usually assigned to the periodicity parallel and perpendicular to the PANI chains, respectively.[42–45] In the spectra of microspheres, these two diffraction peaks are relatively intense, indicating that a crystalline region dispersed in amorphous medium of EB.[46] The crystalline degrees of urchin-like microspheres and smooth microspheres were calculated as 28.86% and 34.23%, respectively, using the XRD processing software.

The differences among the XRD spectra (reflecting the aggregation structure) of three kinds of products can be correlated to pH profiles in their synthetic systems. The quickly dropped pH profile in system *a* accompanies a rapid polymerization rate as well as significantly changed medium condition, which may disturb the self-assembly of PANI with DTPA and the ordered align of PANI molecular chains, so NT and NP obtained in system *a* display a much amorphous structure (Figure 6). During the polymerization courses of systems *b* and *c*, the acidity just slowly changed, which provide a much moderate environment beneficial for the self-assembly and ordered align of PANI molecular chains. It is rational that smooth microspheres obtained in system *c* with nearly a constant pH display the highest crystallinity. Therefore, besides the directing role of a "soft template," the pH profile also has significant effects on the aggregation structures of PANI micro/nanostructures.

Properties

It is interesting to find that by simply adjusting the pH profiles and molar ratio of aniline to DTPA, there are versatile chances to develop the performance of PANI. Four-point probe

Table II. Quantitative Area Ratio Analysis of N1s Peak Components

Chemical environment (eV)	$-^{+}NH_2-$ (403.28)	$-^{+}NH^{-}$ (401.88)	$-N^{+}$ (400.68)	$-NH^{-}$ (399.74)	$-N=$ (398.48)	$-\underset{\vert}{N}-$ (397.88)	N^{+}/N (%)
NT and NP	6.99	6.50	10.11	63.62	12.78	-	23.60
Urchin-like microspheres	5.89	10.48	-	74.18	4.84	4.61	16.37
Smooth microspheres	4.70	16.19	-	74.97	4.14	-	20.89

measurement showed that the NT and NP product has a conductivity of 6×10^{-4} S/cm, which is nearly four orders of magnitude lower than the conventional PANI.[47] The low conductivity of NT and NP can be attributed to lack of aggregated nanogranules on the surface of nanorods or nanotubes forming a textured structure, as proposed by Laslau *et al.*[48] Conductivities of urchin-like microspheres and smooth microspheres were even lower than the detection limit of our four-point probe (1×10^{-4}) S/cm and cannot be exactly measured, probably due to conjugation defects in the PANI backbone and their low doping degree (Table II).

In spite of their similar elemental composition and chemical structures, the three kinds of PANI micro/nanostructures displayed distinct water wettability. The NT and NP is highly hydrophilic, which can quickly absorb a water droplet on its surface and it is rather difficult to record the CA value. As a comparison, the urchin-like microspheres and smooth microspheres show a significant hydrophobic character (Supporting Information, Figure S6), with their measured CAs are as high as 152.3° and 143.5°, respectively.

It can be explained as the NT and NP product with a much higher protonation degree as well as less conjugation defects is intrinsically more hydrophilic than the microsphere products. Moreover, the nanotube and nanoparticle morphology also provides mixed nano- and micro-meter scale roughness which further contributes to their super-hydrophilicity.[49] In the case of microspheres, since only a very small amount of branched units with hydrophobic nature exist in the PANI constructing microspheres (based on FTIR and XPS analysis), the hydrophobic character of those microspheres can be mainly attributed to their roughness surface texture. Therefore, it is necessary to mention that based on the self-assembled micro/nanostructures, the superhydrophobic effect has been achieved using PANI even without introducing components with low surface energy, such as fluorine-containing components.[50]

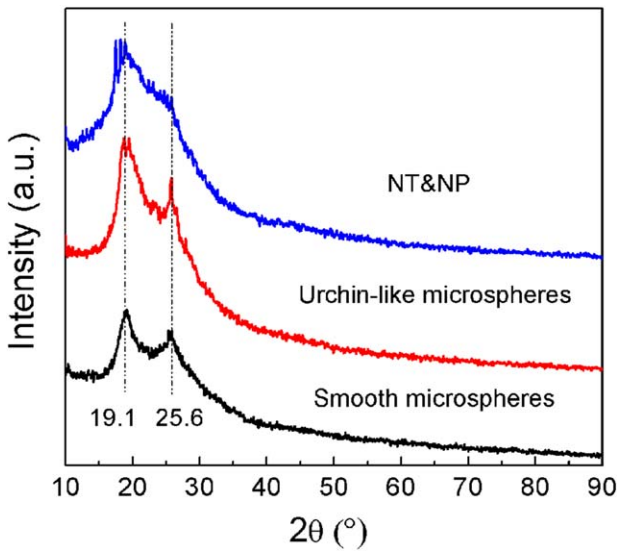

Figure 6. XRD patterns of as-synthesized products at different [Ani]s and [Ani]/[DTPA] ratios. NT and NP: [Ani] = 0.06 M and [Ani]/[DTPA] = 5 : 1; urchin-like microspheres: [Ani] = 0.01 M and [Ani]/[DTPA] = 5 : 1; smooth microspheres: [Ani] = 0.007 M and [Ani]/[DTPA] = 1 : 1. [Color figure can be viewed in the online issue, which is available at wileyonlinelibrary.com.]

Adsorption experiment of Cr (VI) was carried out to further manifest the performance differences among the three kinds of PANI micro/nanostructures. As shown in Table III, the as-synthesized NT and NP product displayed the highest removal percentage in Cr (VI) aqueous solution with concentration of 25 ppm and pH of 1, corresponding to an adsorption capacity of *ca* 20 mg/g, which is much higher than some reference data.[19] By using the microsphere samples as the adsorbent, the removal percentage decreased a little (Table III).

It has been shown by Wang *et al.*[16] that protonated imine groups are the main adsorption sites for Cr (VI) ions below pH = 6.0 and electrostatic interaction is the primary adsorption mechanism. Therefore, the NT and NP products obtained at a lower pH level possessing a higher protonation degree exhibit the best adsorption ability to Cr (VI) ions (Tables II and III). When the microsphere samples were used as the adsorbents, on one hand, since they were mainly obtained at a pH level higher than 2.5 (Figure 2) and possessed lower protonation degree, i.e., a lower percentage of protonated imine groups as compared with the NT and NP sample, thus provided less adsorptions sites for Cr (VI) ions; on the other hand, the highly

Table III. Final Concentration of Cr (VI) and the Corresponding Removal Percentage

Sample	C_f (ppm)	*R* (%, as-synthesized)	*R* (%, redoped)
NT and NP	6.81	74.58	85.89
Urchin-like microspheres	15.96	40.50	53.65
Smooth microspheres	8.50	68.29	81.98

The initial concentration of Cr (VI) is 25 ppm.

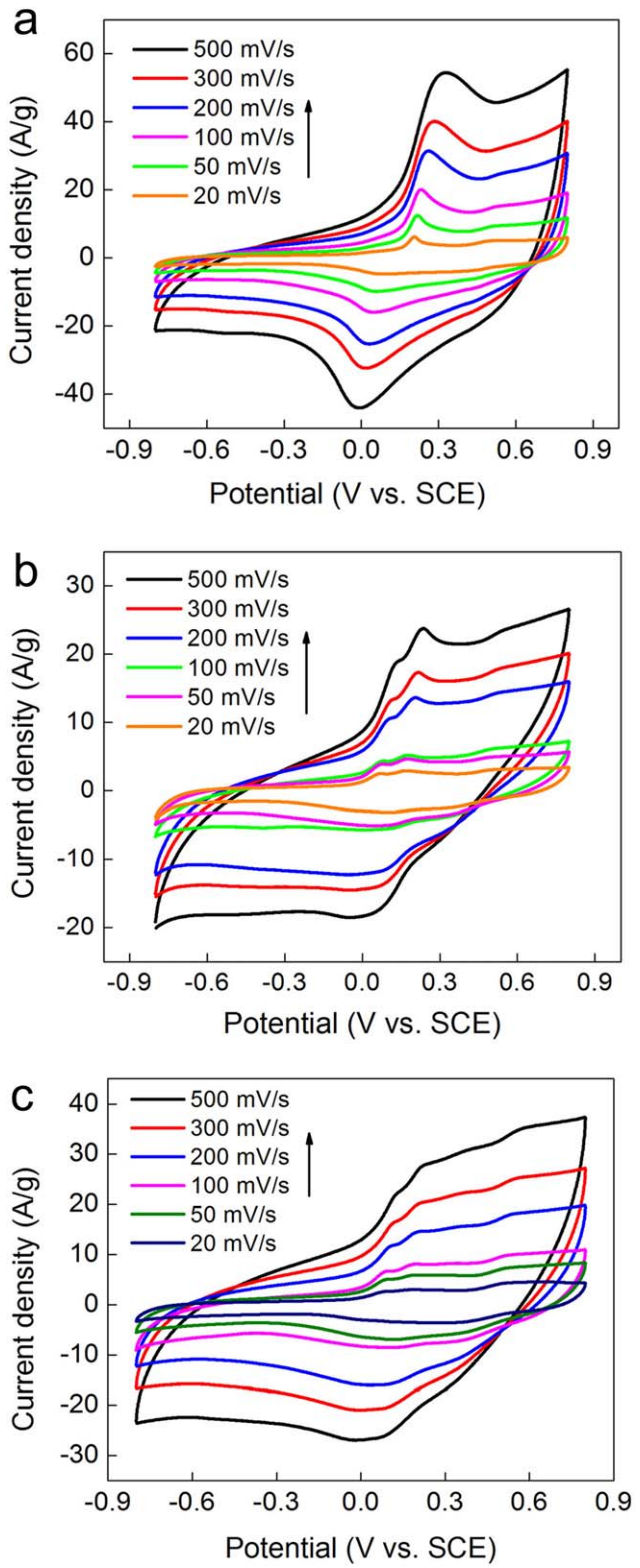

Figure 7. CV curves of the (a) NT and NP, (b) urchin-like microspheres, and (c) smooth microspheres. [Color figure can be viewed in the online issue, which is available at wileyonlinelibrary.com.]

hydrophobic microspheres may not contact sufficiently with the aqueous Cr (VI) ions. So, the microsphere samples display lower Cr (VI) ion removal percentage. Probably due to the less hydrophobic nature of smooth microspheres than urchin-like microspheres, the former one exhibits much strong adsorption ability for Cr (VI) ions.

Considering that the as-synthesized PANI micro/nanostructures actually contain a very low amount of DTPA (as shown in structural analysis section), they were redoped with DTPA and used as adsorbents. Interestingly, the removal percentage for all the redoped samples was obviously increased, especially for the urchin-like microspheres, a 32.5% increase was achieved. This can be attributed to strengthened electrostatic interaction between PANI and Cr (VI) oxyanions[16] as well as increased amount of DTPA which is a strong chelating agent. Though effects of the initial concentration, pH of the Cr (VI) solution, contact time, and doping degree of PANI on the adsorption performance still need further investigation, the present results reflect a promising application potential for removal of Cr (VI) using PANI micro/nanostructures doped with DTPA.

The NT and NP products display better electrochemical behaviors as compared with the two kinds of microspheres, which again reflects their chemical structure and morphology differences. As shown in Figure 7, the CV curves of NT and NP have one couple of redox peaks at 0.32 and −0.01 V, corresponding to transformation of emeraldine salt form to the pernigraniline form and *vice versa*. The CV curves show similar shape, except for increasing current density with increasing scan rate, indicating its good rate capability. The microsphere samples displayed CV curves having redox peaks with much lower current intensity, and an additional small oxidation peak at *ca* 0.11 V appeared beside the one around 0.3 V, which can be attributed to transformation from leucoemeraldine to the conducting state of PANI, while the corresponding redox peak cannot be observed. This character indicates that these urchin-like microspheres and smooth microspheres possess more reduction units than NT and NP, and have been oxidized during CV test with an anodic current while cannot be further reduced.

The specific capacitance of these samples was evaluated by carrying out the galvanostatic charge/discharge measurement with voltage range determined from the CV curves. A group of typical charge/discharge profiles at a current density of 0.5 A/g was given in Figure 8. The discharging time increased in the order of urchin-like microspheres < smooth microspheres < NT and NP, whereas the drop of voltage at the beginning of each discharge curve, which relates to the internal resistance decreased in the same order. The NT and NP, smooth microspheres, and urchin-like microspheres exhibit specific capacitance of 396.5, 306.3, and 228.6 F/g at the current density of 0.5 A/g, respectively [Figure 8(b)]; and the capacitance decreased with the increasing charge current density.

In comparison with the microsphere samples, it is probable that the strong hydrophilicity and a higher conductivity of NT and NP both contribute to their high specific capacity. However, the circulation stabilities of the samples were very poor; even for the NT and NP sample, nearly 50% of the original specific capacitance was lost after 100 times of charge–discharge. As the charge–discharge process was carried out in 1 M H_2SO_4, repeated doping and dedoping due to electrolyte insertion and

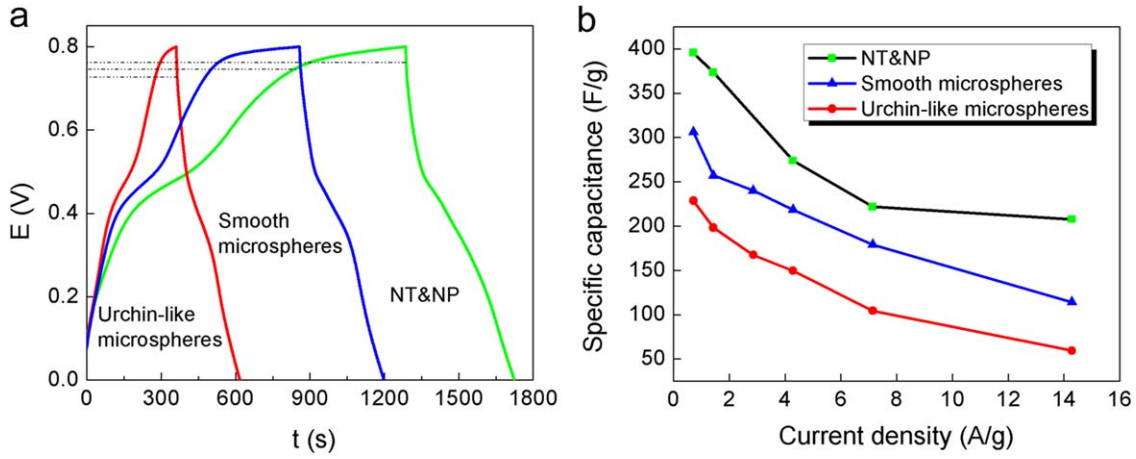

Figure 8. (a) Glavanostatic charge/discharge profiles recorded at a current density of 0.5 A/g and (b) specific capacitance obtained with different current densities for the three kinds of typical PANI micro/nanostructures. [Color figure can be viewed in the online issue, which is available at wileyonlinelibrary.com.]

extraction will induce expansion and shrink of the polymer backbone which is difficult to recover. Though the present PANI micro/nanostructures are not ideal candidates for high-performance supercapacitor electrode materials, their distinct electrochemical behaviors further demonstrate a comprehensive performance differences determined by their chemical structures and aggregation structures.

CONCLUSIONS

By carrying out aniline COP in DTPA solution with specific pH profiles, PANI nanotubes accompanied with nanoparticles (NT and NP), urchin-like microspheres, and smooth microspheres were obtained. The as-produced PANI micro/nanostructures are mainly doped with sulfonic acid and the existence of DTPA in the final products is hardly to detect. In the COP system with quickly dropped pH, effect of "soft template" on construction of PANI micro/nanostructures is not obvious. The appearance of semicurled nanotubes gives a direct support for the nanosheet curling mechanism of PANI nanotube formation. In the COP systems with slowly changed pH in the early reaction stage, DTPA with steric configuration may be helpful for formation of 3-D nucleation center which consequently results in urchin-like microspheres or smooth microspheres corresponding to acidity levels below 2.5 and slightly above 2.5, respectively. The NT and NP products possess a higher protonation degree and a strong hydrophilic nature, which bring in a good adsorption performance for Cr (VI) ions and electrochemical response with a specific capacitance high to 398 F/g at a current density of 0.5 A/g. Probably due to hydrophobic molecular structure and unique surface texture, the microsphere samples show significant superhydrophobic property, which consequently weakens their adsorption ability to Cr (VI) ions and lead to poor electrochemical behaviors. This work provides a sight to evaluate the contribution of "soft template" and pH profiles on the products from aniline COP system, which will be helpful for carrying out efficient morphology control and performance enhancement of PANI micro/nanostructures.

ACKNOWLEDGMENTS

The work was supported by the Fundamental Research Funds for the Central Universities (No. XJJ 2014008) and the China Postdoctoral Science Foundation (No. 2013M532037). The SEM work was done at International Center for Dielectric Research (ICDR), Xi'an Jiaotong University. The authors also thank Ms. Dai Yanzhu for her help in using SEM.

REFERENCES

1. Cao, Y.; Smith, P.; Heeger, A. *J. Synth. Met.* **1993**, *57*, 3514.
2. Huang, W.-S.; Humphrey, B. D.; MacDiarmid, A. G. *J. Chem. Soc., Faraday Trans.* **1986**, *82*, 2385.
3. Stejskal, J.; Sapurina, I.; Trchová, M.; Konyushenko, E. N. *Macromolecules* **2008**, *41*, 3530.
4. Venancio, E. C.; Wang, P. C.; MacDiarmid, A. G. *Synth. Met.* **2006**, *156*, 357.
5. Stejskal, J.; Trchová, M. *Polym. Int.* **2012**, *61*, 240.
6. Zhao, Y.; Tomšík, E.; Wang, J.; Morávková, Z.; Zhigunov, A.; Stejskal, J.; Trchová, M. *Chem. Asian J.* **2013**, *8*, 129.
7. Trchová, M.; Šedenková, I.; Konyushenko, E. N.; Stejskal, J.; Holler, P.; Ciric-Marjanovic, G. *J. Phys. Chem. B* **2006**, *110*, 9461.
8. Sapurina, I.; Stejskal, J. *Polym. Int.* **2008**, *57*, 1295.
9. Li, Y.; Wang, Y.; Jing, X.; Zhu, R. *J. Polym. Res.* **2011**, *18*, 2119.
10. Jin, E.; Wang, X.; Liu, N.; Zhang, W. *Mater. Lett.* **2007**, *61*, 4959.
11. Wang, H.; Lu, Y. *Synth. Met.* **2012**, *162*, 1369.
12. Wan, M. *Macromol. Rapid Commun.* **2009**, *30*, 963.
13. Trchova, M.; Sedenkova, I.; Konyushenko, E. N.; Stejskal, J.; Holler, P.; Ciric-Marjanovic, G. *J. Phys. Chem. B* **2006**, *110*, 9461.
14. Šeděnková, I.; Trchová, M.; Stejskal, J.; Bok, J. *Appl. Spectrosc.* **2007**, *61*, 1153.

15. Zujovic, Z. D.; Zhang, L.; Bowmaker, G. A.; Kilmartin, P. A.; Travas-Sejdic, J. *Macromolecules* **2008**, *41*, 3125.
16. Wang, J.; Zhang, K.; Zhao, L. *Chem. Eng. J.* **2014**, *239*, 123.
17. Krishnani, K. K.; Srinives, S.; Mohapatra, B.; Boddu, V. M.; Hao, J.; Meng, X.; Mulchandani, A. *J. Hazard. Mater.* **2013**, *252*, 99.
18. Guo, X.; Fei, G. T.; Su, H.; De Zhang, L. *J. Phys. Chem. C* **2011**, *115*, 1608.
19. Eisazadeh, H. *J. Appl. Polym. Sci.* **2007**, *104*, 1964.
20. Bhaumik, M.; Maity, A.; Srinivasu, V.; Onyango, M. S. *Chem. Eng. J.* **2012**, *181*, 323.
21. Stejskal, J.; Sapurina, I.; Trchová, M. *Prog. Polym. Sci.* **2010**, *35*, 1420.
22. Li, Y.; He, W.; Feng, J.; Jing, X. *Colloid Polym. Sci.* **2012**, *290*, 817.
23. Sun, J.; Bi, H. *Appl. Surf. Sci.* **2012**, *258*, 4276.
24. Zhang, L.; Peng, H.; Zujovic, Z. D.; Kilmartin, P. A.; Travas-Sejdic, J. *Macromol. Chem. Phys.* **2007**, *208*, 1210.
25. Rezaei, S. J. T.; Bide, Y.; Nabid, M. R. *Synth. Met.* **2011**, *161*, 1414.
26. Huang, Y.; Lin, C. *Polymer* **2009**, *50*, 775.
27. Zujovic, Z. D.; Laslau, C.; Bowmaker, G. A.; Kilmartin, P. A.; Webber, A. L.; Brown, S. P.; Travas-Sejdic, J. *Macromolecules* **2010**, *43*, 662.
28. Laslau, C.; Zujovic, Z.; Travas-Sejdic, J. *Prog. Polym. Sci.* **2010**, *35*, 1403.
29. Rozlívková, Z.; Trchová, M.; Šeděnková, I.; Špírková, M.; Stejskal, J. *Thin Solid Films* **2011**, *519*, 5933.
30. Li, Y.; Wang, B.; Feng, W. *Synth. Met.* **2009**, *159*, 1597.
31. Sedenkova, I.; Trchova, M.; Blinova, N. V.; Stejskal, J. *Thin Solid Films* **2006**, *515*, 1640.
32. Zhang, L.; Long, Y.; Chen, Z.; Wan, M. *Adv. Funct. Mater.* **2004**, *14*, 693.
33. Laslau, C.; Zujovic, Z. D.; Zhang, L.; Bowmaker, G. A.; Travas-Sejdic, J. *Chem. Mater.* **2009**, *21*, 954.
34. Monkman, A.; Stevens, G.; Bloor, D. *J. Phys. D: Appl. Phys.* **1991**, *24*, 738.
35. Golczak, S.; Kanciurzewska, A.; Fahlman, M.; Langer, K.; Langer, J. J. *Solid State Ionics* **2008**, *179*, 2234.
36. Mu, S. L. *Macromol. Chem. Phys.* **2005**, *206*, 689.
37. Jousseaume, V.; Morsli, M.; Bonnet, A. *J. Appl. Polym. Sci.* **2003**, *90*, 3730.
38. Wei, X.-L.; Fahlman, M.; Epstein, A. *Macromolecules* **1999**, *32*, 3114.
39. Surwade, S. R.; Dua, V.; Manohar, N.; Manohar, S. K.; Beck, E.; Ferraris, J. P. *Synth. Met.* **2009**, *159*, 445.
40. Konyushenko, E. N.; Stejskal, J.; Šeděnková, I.; Trchová, M.; Sapurina, I.; Cieslar, M.; Prokeš, J. *Polym. Int.* **2006**, *55*, 31.
41. Chan, H.; Ng, S.; Sim, W.; Seow, S.; Tan, K.; Tan, B. *Macromolecules* **1993**, *26*, 144.
42. Pouget, J. P.; Jdzefowicz, M. E.; Epstein, A. J.; Tang, X.; MacDiarmid, A. G. *Macromolecules* **1991**, *24*, 779.
43. Lee, K.; Cho, S.; Park, S. H.; Heeger, A. J.; Lee, C. W.; Lee, S. H. *Nature* **2006**, *441*, 65.
44. Rahy, A.; Yang, D. J. *Mater. Lett.* **2008**, *62*, 4311.
45. Chaudhari, H.; Kelkar, D. *J. Appl. Polym. Sci.* **1996**, *62*, 15.
46. Lee, K.; Cho, S.; Park, S. H.; Heeger, A.; Lee, C.-W.; Lee, S.-H. *Nature* **2006**, *441*, 65.
47. Jing, X.; Wang, Y.; Wu, D.; Qiang, J. *Ultrason. Sonochem.* **2007**, *14*, 75.
48. Laslau, C.; Zujovic, Z. D.; Travas-Sejdic, J. *Macromol. Rapid Commun.* **2009**, *30*, 1663.
49. Darmanin, T.; Guittard, F. *Prog. Polym. Sci.* **2014**, *39*, 656.
50. Zhu, Y.; Hu, D.; Wan, M.; Jiang, L.; Wei, Y. *Adv. Mater.* **2007**, *19*, 2092.